Internal Series Resistance in Cu(In,Ga)Se$_2$ Solar Cells Analysed by Electroluminescence

Uwe Rau, Vito Huhn, and Bart E. Pieters
IEK5-Photovoltaik, Forschungszentrum Jülich, 52425 Jülich, Germany

Supplementary Information

I. SCAPS Simulations

This supplementary information describes how the SCAPS simulations were fitted to the experimental results. The simulations are based on the parameter set taken from [1,2]. The parameters for the CIGS absorber and CdS buffer layer are given in Table 1 and 2. In the simulations the bandgap is graded from 1.36 eV at the back contact to 1.18 eV at the CdS interface. The electron affinity varies accordingly to allow for a constant valence band position, i.e. over the absorber it holds that $\boldsymbol{\chi + E_g = \text{const.}}$, where both $\boldsymbol{\chi}$ and $\boldsymbol{E_g}$ vary linearly. The contact TCO layers are neglected in the simulations.

Table 1: Simulation parameters: layer properties

	CIGS	CdS
Thickness d [µm]	1.92	0.06
Bandgap E_g [eV]	$1.36 - 1.1808$	2.4
Electron Affinity χ [eV]	$4.2 - 4.3680$	4.27
Relative Permittivity ϵ_r [r.u.]	13.6	10
Density of States N_C [cm^{-3}]	2.2×10^{18}	2.2×10^{18}
Density of States N_V [cm^{-3}]	1.8×10^{19}	1.8×10^{19}
Thermal Velocity v_{th} [cm/s]	10^7	10^7
Electron Mobility[1] μ_e [cm^2/Vs]	60	100
Hole Mobility μ_h [cm^2/Vs]	5	25
Doping Density[1] $N_{A/D}$ [cm^{-3}]	4.9×10^{16}	5×10^{17}
Radiative Recombination Constant B [cm^{-3}/s]	2×10^{-9}	0

For the simulation of illuminated experiments the excitation wavelength was set to 800 nm (similar to the experimental conditions) and the intensity was adjusted to 580 W/m² to have roughly the short circuit current that was measured in the experiment. Furthermore, the external series resistance was set to 3.5 $\Omega\mathrm{cm}^2$.

As a first step of the fitting process, outgoing from the base parameter set, different parameters were varied and the effects on the *J/V*-characteristics and the internal voltage analyzed. The internal voltage is determined within the SCAPS simulations similar to the experiment. The total radiative recombination is determined from the electron and hole charge carrier density and

[1]These parameters are later adjusted to fit the model to the experimental results.

calibrated towards an internal voltage with the radiative recombination under open circuit conditions.

Note that the internal voltage is calculated from the radiative recombination current J_{rad} in the CIGS absorber layer provided by SCAPS, using $qV_{\text{int}} = qV_{OC} - kT \log\{J_{rad}(V_{OC}) / J_{rad}(V_{ext})\}$, i.e. we scale the values at each to the open circuit situation. This is the same procedure as that one we are using to scale the experimental data.

Table 2: Simulation parameters: defects

	CIGS	CdS
Type	Donor	Acceptor
Capture Cross Section σ_e [cm^2]	10^{-14}	8×10^{-17}
Capture Cross Section σ_h [cm^2]	10^{-14}	8×10^{-12}
Defect Position E_T [eV]	0.094 below Conduction Band	at intrinsic Fermi Energy
Characteristic Energy of Defect Distribution σ_T^E [eV]	0.018	0.1
Peak Defect Density N_T [$eV^{-1}cm^{-3}$]	3.16×10^{16}	4.514×10^{17}
Type	Acceptor	
Capture Cross Section σ_e [cm^2]	3×10^{-14}	
Capture Cross Section σ_h [cm^2]	10^{-14}	
Defect Position E_T [eV]	0.227 below Conduction Band	
Characteristic Energy of Defect Distribution σ_T^E [eV]	0.05	
Peak Defect Density N_T [$eV^{-1}cm^{-3}$]	1.41×10^{15}	

Exemplarily Figure S1-3 show the influence of the bandgap, the electron mobility and the doping density of the CIGS absorber on the J/V characteristics and internal voltage. Bandgap variations mainly influence the open circuit voltage (Fig. S1a) and the internal voltage changes mostly linearly with changes in the Bandgap (Fig. S1b). A low mobility of the electrons (minority carriers) in the CIGS bulk leads to loss of photocurrent and leads to a gradient in the *J/V* characteristics at low voltages, which is often called voltage dependent photocurrent (Fig. S2a). Low mobilities also increase the internal voltage at negative currents, but in contrast to changes resulting from Bandgap variations the effect is reversed at positive currents (Fig. S2b). Low doping densities on the other hand increase the short circuit current and decrease the open circuit voltage (Fig. S3). Low doping densities also decrease the internal voltage. Furthermore changes in the doping density have the potential to change the gradient of the internal voltage with the external voltage.

To fit the SCAPS simulations to the experimental results it was made use of these findings. The doping and the electron mobility was manually iteratively adjusted to be able to reproduce on the one hand the gradient of the internal voltage with external voltage (by significantly lowering the **doping density to 2.1×10^{15} cm^{-3}**) and, on the other hand, the gradient of the current with external voltage at low voltages under illumination (by lowering the **electron mobility to 3 cm^2/Vs**). In the end additionally the illumination intensity had to be adjusted slightly to 540 W/m² to fit the short circuit current of *J/V* characteristic. The final fit is shown in Fig. S4 together with the experimental results. The other parameters were kept equal to the one in Table 1.

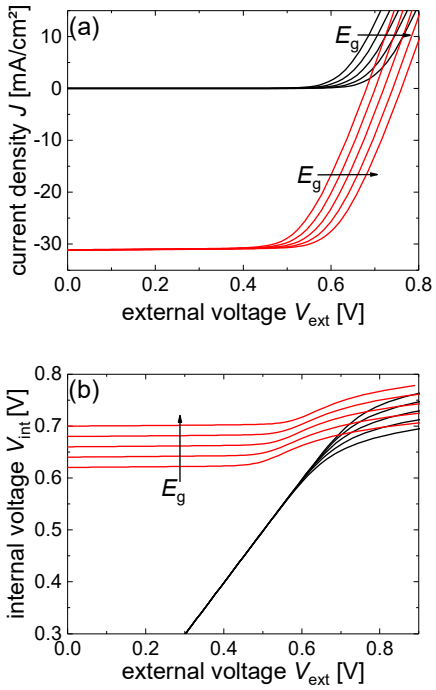

Fig S1. *J/V* characteristics (a) and internal voltage plotted against the external voltage (b) for varying bandgaps. Black: without illumination. Red: under illumation. Lowest Bandgap rising from 1.1208 eV to 1.2008 eV in 0.02 eV steps. A larger Bandgap increases the open circuit voltage. Furthermore, the internal voltage increases linearly with the bandgap at all external voltages.

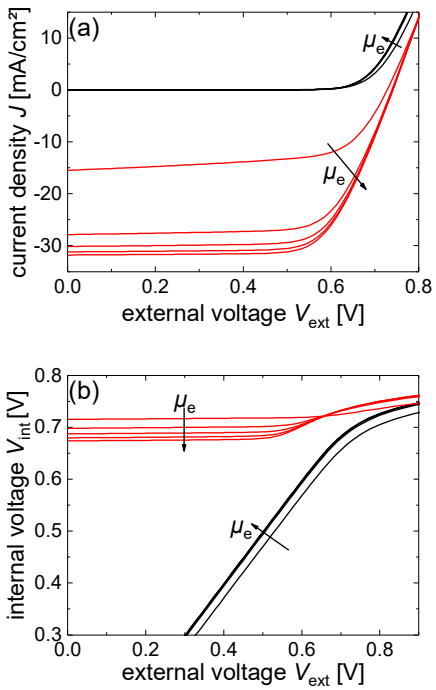

Fig S2. *J/V* characteristics (a) and internal voltage plotted against the external voltage (b) for varying electron mobilities. Black: without illumination. Red: under illumation. Electron mobility rising from 1 cm^2/Vs to 81 cm^2/Vs in 20 cm^2/Vs steps. Higher mobilites lead to larger currents under illumination and lower internal voltages under illumination and low external voltages. Furthermore, the mobility influences the gradient of the *J/V* characteristics at low external voltages.

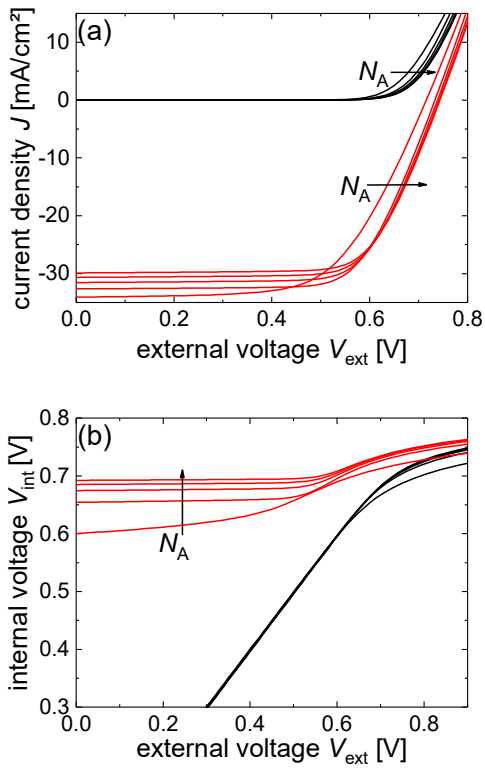

Fig S3. *J/V* characteristics (a) and internal voltage plotted against the external voltage (b) for varying doping densities. Black: without illumination. Red: under illumation. Doping density rising from 0.1×10^{16} cm^{-3} to 8.1×10^{16} cm^{-3} in 2×10^{16} cm^2/Vs steps. Low doping densities increase the short circuit current and decrease the open circuit voltage. A lower doping density decreases the internal voltage and may lead to a more significant gradient of the internal voltage at low external voltages.

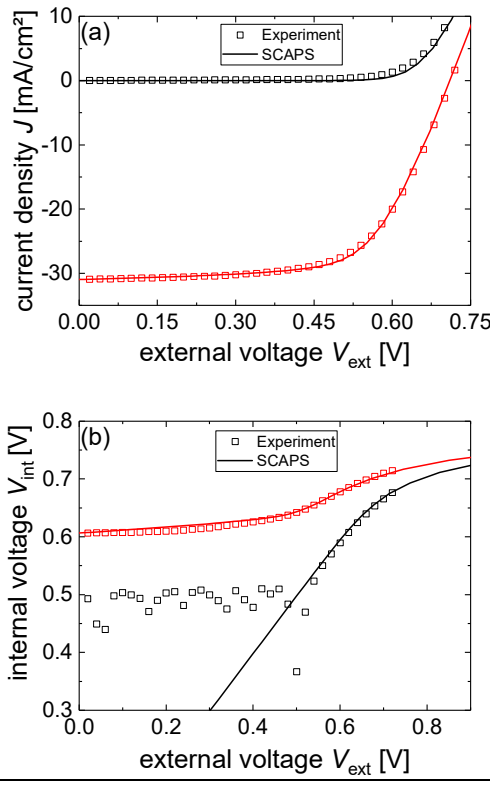

Fig S4. *J/V* characteristics (a) and internal voltage plotted against the external voltage (b). Comparisaon of experimental results (squares) and SCAPS simulation. Black: without illumination. Red: under illumation.

II. Validity of Eqs. (16) and (17) in case of non-ideal recombination $n_{id} \neq 1$

We solve Eq. (8)

$$J_B\left[\exp\left(\frac{qV_{\text{int}}}{kT}\right)-\exp\left(\frac{qV_{ext}}{kT}\right)\right]=J_L-J_0\left[\exp\left(\frac{qV_{\text{int}}}{n_{id}kT}\right)-1\right] \tag{8}$$

numerically in order to derive the interdependence $V_{\text{int}}(V_{ext})$ of the internal on the external voltage. With this the external current voltage characteristics $J(V_{ext})$ is known and the residual internal short circuit V_{int}^{SC} as well as the loss $\Delta J_{SC}=J_L-J_{SC}=J_L-J(V_{ext}=0)$ is calculated. Note that the saturation current density J_0 for different ideality factors is calculated from the fixed open circuit voltage

$$J_0=\frac{J_L}{\exp\left(\frac{qV_{OC}}{n_{id}kT}\right)-1}. \tag{S1}$$

Figure S5 demonstrates the validity of the approximations given by Eq.(16) and (17) for ideality factors n_{id} between 1 and 2 for a range of reference current densities $J_B > 10^{-9}$ mAcm^{-2}. Note that with smaller values of J_B, V_{int}^{SC} approaches V_{OC} and the short circuit current loss ΔJ_{SC} approaches J_{SC} such that the device becomes extremely poor concerning its abilities of charge carrier separation.

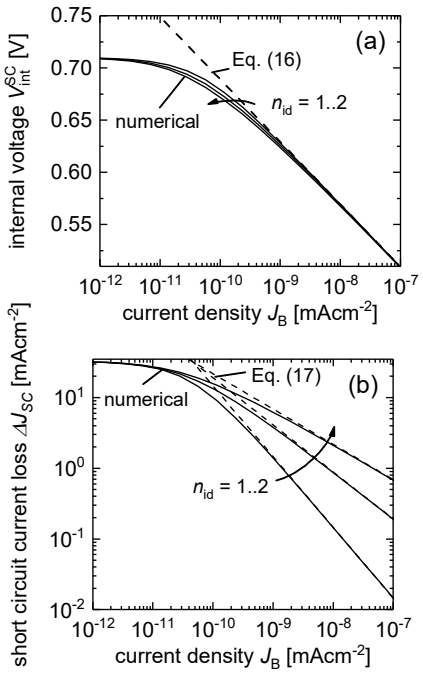

Fig. S5 (a) Dependence of the residual internal short circuit voltage V_{int}^{SC} on the reference current density J_B for ideality factors n_{id} = 1, 1.5, and 2. (b) Dependence of the short circuit current loss ΔJ_{SC} on the reference current density J_B. The analytical approximations given by Eqs. (16) and (17) are valid for $J_B > 10^{-9}$ mAcm^{-2}.

III. Violation of the Wong-Green network theorem - Derivation of Eq. (19) and (20)

Reorganizing Eq. (15) leads to

$$V_{ext} = V_{\mathrm{int}} + R_S(V_{\mathrm{int}})J\,. \tag{S2}$$

The derivative of Eq. (S2)

$$\frac{dV_{ext}}{dV_{\mathrm{int}}} = 1 + \frac{dJ}{dV_{\mathrm{int}}}R_S + J\frac{dR_S}{dV_{\mathrm{int}}} \tag{S3}$$

leads to Eq. (19). The derivative of the terminal current J with respect to the short circuit current J_L (under constant V_{ext}) leads to

$$-\frac{dJ}{dJ_{SC}} = 1 - \frac{dJ}{dV_{\mathrm{int}}}\frac{dV_{\mathrm{int}}}{dJ_L}\,. \tag{S4}$$

From Eq. (S2) we obtain

$$\frac{dV_{\mathrm{int}}}{dJ_L} = -J\frac{dR_S}{dV_{\mathrm{int}}}\frac{dV_{\mathrm{int}}}{dJ_L} - \frac{dJ}{dJ_L}R_S \quad . \tag{S5}$$

Setting Eq. (S5) into Eq. (S4) leads to

$$-\frac{dJ}{dJ_L}\left(1 + \frac{dR_S}{dV_{\mathrm{int}}}J\right) = 1 + \frac{dR_S}{dV_{\mathrm{int}}}J + R_S\frac{dJ}{dV_{\mathrm{int}}}\frac{dJ}{dJ_L} \tag{S5}$$

which by reorganization finally leads to Eq. (20).

IV. Superposition of short circuit photoluminescence and electroluminescence

We assume that the luminescence Φ is determined by the internal voltage V_{int} via the proportionality

$$\Phi \sim \left\{\exp\left(\frac{qV_{\mathrm{int}}}{kT}\right) - 1\right\}. \tag{S6}$$

Reorganizing Eq. (9) and the use of Eq. (S7) leads to

$$\Phi \sim \left\{\exp\left(\frac{qV_{\mathrm{int}}}{kT}\right) - 1\right\} = \frac{J_B}{J_B + J_0}\left\{\exp\left(\frac{qV_{ext}}{kT}\right) - 1\right\} + \frac{J_L}{J_B + J_0}\,. \tag{S7}$$

With Eq. (S7) the luminescence emission is a superposition of a term that is exponentially driven by the external voltage V_{ext} and a residual (short circuit) term that is driven by the photogenerated current J_L, in analogy to Ref. [3].

V. Ratio between short circuit and open circuit luminescence

From Eq. (S7) we have under short circuit conditions

$$\Phi_{SC} \sim \frac{J_L}{J_B + J_0} \tag{S8}$$

and under open circuit

$$\begin{aligned} \Phi_{OC} &\sim \frac{J_B}{J_B + J_0}\left\{\exp\left(\frac{qV_{ext,OC}}{kT}\right) - 1\right\} + \frac{J_L}{J_B + J_0} \\ &= \frac{J_B}{J_B + J_0}\frac{J_L}{J_0} + \frac{J_L}{J_B + J_0} = \frac{(J_B + J_0)J_L}{(J_B + J_0)J_0} = \frac{J_L}{J_0} \end{aligned}. \tag{S9}$$

Thus, the ratio between short circuit and open circuit luminescence reads

$$\frac{\Phi_{SC}}{\Phi_{OC}} = \frac{J_0}{J_B + J_0}. \tag{S10}$$

Considering Eq. (11), the short circuit current J_{SC} is reduced with respect to the photogenerated current by

$$\Delta J_{SC} = J_L - J_{SC} = J_L\left(1 - \frac{J_B}{J_0 + J_B}\right) = J_L\frac{J_0}{J_0 + J_B}. \tag{S11}$$

By comparing Eq. (S10) and (S11) we find

$$\frac{\Phi_{SC}}{\Phi_{OC}} = \frac{\Delta J_{SC}}{J_L}. \tag{S12}$$

Thus, the easily measurable luminescence ratio gives a direct measure for the losses in short circuit current. Equation (S12) is however only valid if recombination follows a diode law with an ideality factor $n_{id} = 1$. For ideality factors $n_{id} \neq 1$ we find from the approximations given by Eqs. (16) and (17) the more general expression

$$\frac{\Phi_{SC}}{\Phi_{OC}} = \left(\frac{\Delta J_{SC}}{J_L}\right)^{n_{id}}. \tag{S13}$$

---

1 J. F. L. Salas, S. J. Heise, M. Richter, V. Gerliz, M. S. Hammer, J. Ohland, I. Hammer-Riedel, Simulation of metastable changes in time resolved photoluminescence of Cu(In,Ga)Se_2 thin film solar cells upon light soaking treatment, Thin Solid Films **633**, 40 (2016).

2 S. J. Heise, V. Gerliz, M. S. Hammer, J. Ohland, J. Keller, and I. Hammer-Riedel, Light-induced changes in the minority carrier diffusion length of Cu(In,Ga)Se_2 absorber material, Sol. Ener. Mat. Sol. Cells **163**, 270 (2017).

3 U. Rau, IEEE J. Photovoltaics **2**, 169 (2012).